Acta Astronautica 154 (2019) 103–118

Contents lists available at ScienceDirect

Acta Astronautica

journal homepage: www.elsevier.com/locate/actaastro

BELA transmitter performance and pointing stability verification campaign at DLR-PF

C. Althaus*, H. Michaelis, H. Hussmann, K. Lingenauber, R. Kallenbach, S. Del Togno, F. Lüdicke

Deutsches Zentrum für Luft- und Raumfahrt e.V., Rutherfordstr. 2, 12489, Berlin, Germany

ARTICLE INFO

Keywords:
Mercury
BELA
BepiColombo
Laser altimeter
Transmitter
Verification

ABSTRACT

BELA is the first European planetary laser altimeter and shall be launched onboard of ESA's Mercury Planetary Orbiter (MPO) as part of the BepiColombo spacecraft in October 2018. The complete development of the instrument was done in collaboration with team members in Switzerland, Germany and Spain. The transmitter is also the first space-qualified laser system for a planetary mission built in Europe. Highly important for scientific performance is the transmitter's performance which is specified with demanding values. Thermo-optical pointing stability, alignment, pulse energy, wavelength, pulse profile and length have a direct impact on the signal quality and strength of the instrument and in consequence on the quality of science data. Furthermore for in-orbit operation the detailed knowledge of the transmitter behavior is required for the interpretation of measurement data. Therefore the transmitter, an encapsulated diode pumped pulsed Nd:YAG laser, was extensively tested at facilities at DLR in Berlin-Adlershof under various environmental conditions in all possible representative configurations. This is necessary because thermo-elastic and optical behavior are difficult to predict accurately only theoretically. Furthermore there are temperature dependent effects, e.g. for laser energy, which directly affect science measurements and can only be calibrated on-ground. An optical test bench was designed and set up for this particular task. This work describes the test bench and the measurement procedures. The measurement results for the Engineering Qualification Model and Flight Model are presented and discussed as well as lessons learned. The outcome of the tests shows that the BELA FM transmitter performs well with margins and BELA is expected to achieve its scientific goals.

1. Introduction

The instrument BELA is the first European planetary laser altimeter. It is part of the scientific payload of the Mercury Planetary Orbiter (MPO) of the BepiColombo mission scheduled for launch in October 2018. The main science objectives after orbit insertion end of 2025 are to generate an accurate global topographic map of Mercury as well as determination of tidal shape deformations, librations and obliquity to obtain an understanding of the internal structure of this planet closest to the sun. The orbit will be polar, elliptic by 400 × 1500 km with a 2.3 h period. Nominal operation time is planned with 1 year plus 1 year extension. More details on the mission are described in Refs. [1], [2].

Although BELA will be the second laser altimeter at Mercury after the Mercury Laser Altimeter (MLA) onboard MESSENGER [3], it features some distinct differences. BELA has a powerful digital rangefinder capable of detecting return pulses with an SNR close to 1. It will map both, north and south hemispheres of the planet. And its lasers have with 50 mJ at 10 Hz the highest pulse energy of all flown planetary laser altimeters so far. And in fact the performance of the transmitter laser determines the capabilities of the whole instrument BELA. Laser pulse energy is a function of temperature, emitted light wavelength of the laser diode arrays. Pulse length and pulse shape, beam divergence, laser beam alignment and pointing stability also depend on temperature, gravity and ambient pressure conditions. Accurate prediction is not possible only by analysis as the system is complex and contains many parameters which are hard to determine. An accurate alignment and high pointing stability is fundamental because the field of view of the receiver telescope is very narrow to limit background noise. The total alignment error budget, including the transmitter's contribution, is 500 μrad. The transmitter has a maximum absolute alignment error of 100 μrad with regard to the receiver and the maximum pointing stability is 50 μrad. This pointing stability includes all deviations to the initial alignment during the mission caused by temperature, vibration, shock, pressure drop to vacuum at launch, gravity release, cruise and

* Corresponding author.
E-mail addresses: christian.althaus@dlr.de (C. Althaus), harald.michaelis@dlr.de (H. Michaelis), hauke.hussmann@dlr.de (H. Hussmann), kay.lingenauber@dlr.de (K. Lingenauber), reinald.kallenbach@dlr.de (R. Kallenbach), simone.deltogno@dlr.de (S. Del Togno), fabian.luedicke@dlr.de (F. Lüdicke).

https://doi.org/10.1016/j.actaastro.2018.09.032
Received 18 May 2018; Received in revised form 31 August 2018; Accepted 27 September 2018
Available online 10 October 2018

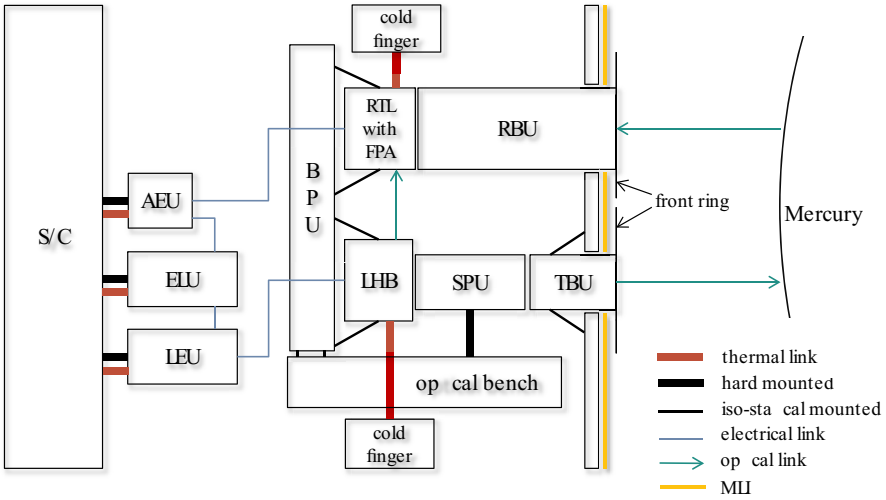

Fig. 1. Functional block diagramme of the complete BELA instrument. It consists of 7 units of which 3 are electronics boxes and 4 are optical and opto-mechanical units. Latter ones are mounted on the optical bench of the spacecraft.

operation and determines where the instrument measures the range. A 50 μrad error causes a shift of 20 to 50 m on the surface due to the distance of 400 to 1000 km of the MPO to the Mercury surface. Therefore the maximum allowed shift of 50 μrad must be guaranteed at all times in order to get useful science data. This is a challenging requirement especially in such a thermal extreme environment as at Mercury. Although the complete instrument BELA was finally integrated and verified at the University of Bern, a verification campaign on the transmitter was performed at DLR Berlin facilities earlier. This was done intentionally to keep the test complexity low and to identify issues as early as possible.

2. Instrument design

2.1. BepiColombo laser altimeter - BELA

BELA is composed of seven units (Fig. 1). These are Baseplate Unit (BPU), on which the transmitter Laser Head Box (LHB) and Receiver Telescope (RTL) are mounted. The BPU is a carbon fiber reinforced honeycomb plate and provides the required opto-mechanical stiffness and stability for the co-alignment and stability of the transmitter line of sight to the receiver line of sight and the absolute alignment with regard to the spacecraft optical bench and star-trackers [1]. Then there are 3 purely electronic units. One of them is the Electronics Unit (ELU) which controls the whole instrument and processes the signals and acquired data. The Laser Electronics Unit (LEU) powers and controls the laser. The Analog Electronics Unit (AEU) amplifies the detector signal and redirects it for digitization to the Range Finder Module (RFM) inside the ELU. Furthermore there are 3 units with optical functions. These are the Receiver Baffle Unit (RBU) which protects the receiver from overheating and straylight, the Transmitter Baffle Unit (TBU) which protects the transmitter analogous and the Straylight and Contamination Protection Unit (SPU) which closes the gap between LHB and TBU [4]. It ensures that no unwanted laser light is emitted which could potentially cause false signals on the receiver side or even damage it. The overall performance of the instrument, i.e. how accurate a range measurement can be done and located on the surface, depends strongly on the properties of the laser beam most importantly pulse energy, shape, duration and pointing [5] (see Fig. 2).

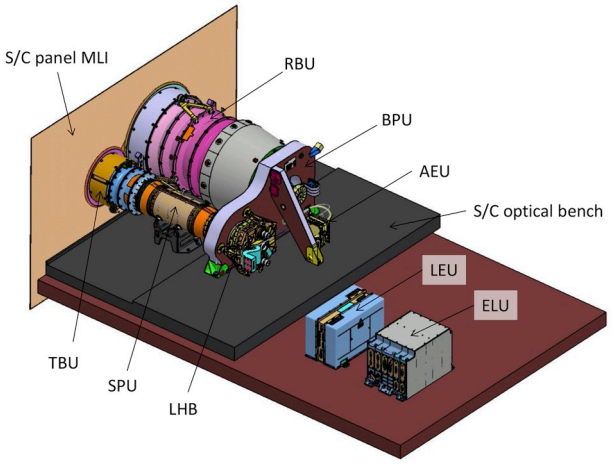

Fig. 2. The BELA instrument with the electronic boxes ELU, LEU and AEU. BPU and S/C panel carry LHB, RTL, FPA, TBU and RBU.

2.2. BELA transmitter

The unit which is subject of the verification is the BELA transmitter. The key parameters are listed in Table 1. It consists of the LEU and the LHB. While the LEU (Laser Electronics Unit) includes the electronics for driving the laser diodes, i.e. the capacitors and the Pockels cell driver, the LHB houses the laser cavity with the laser pump diodes and the Pockels cell itself. For reasons of laser induced damage thresholds and contamination the LHB is hermetically sealed with a metallic c-ring with 1 bar nitrogen. The alignment, i.e. pointing accuracy and the pointing stability of the laser beam are fundamental properties of the LHB. They are affected by internal and external factors, including physical motion, heat buildup and thermal expansion in the housing, cavity instability, air flows (only in the laboratory), vibration, gravity, ageing etc. Hence, the design of the LHB was driven to achieve a high pointing stability. Accurate alignment is ensured by 3 isostatic bipods which minimize the mechanical stress in the LHB. The material of the LHB is AlBeMet which is an alloy from about 62% of aluminum and 38% of beryllium. It is lighter, stiffer, and more thermally stable compared to aluminum and has also a high thermal conductivity to achieve quasi-isothermal behavior [6]. It offers moreover adequate CTE matching with the base plate. The temperature distribution has a critical impact on the pointing stability as well as beam divergence. Internal optical benches in the LHB hold the optical components, back mirrors, laser rods, polarizers, outcoupling mirrors etc. and are mechanically decoupled from the rest of the structure to limit movements

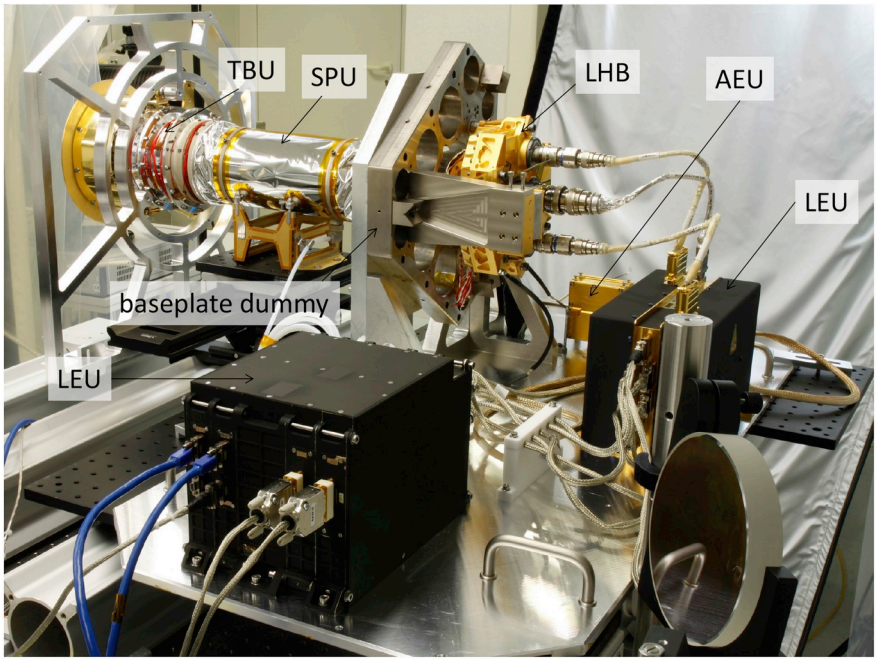

Fig. 3. BELA FM transmitter with integrated SPU and TBU in MGSE configuration. In the foreground the electronics boxes ELU and LEU are shown. The beige cables coming from the LHB are protected with Kynar mantles and provide the 100 A of laser diode pump current.

Table 1
BELA transmitter technical key parameters relevant for scientific performance.

parameter	specified value	unit	remark
wavelength	1064.42 ± 0.25	nm	vacuum wavelength
pulse energy (BOL)	≥ 50	mJ	–
pulse energy (EOL)	≥ 40	mJ	–
pulse energy stability	≤ 2.5	mJ	1 σ
pulse length	5.5 ± 2.5	ns	FWHM
pulse repetition rate	1 … 10	Hz	alterable during operation in steps of 1 Hz for power saving; the nominal pulse repetition rate is 10 Hz though
alignment	≤ 100	*µrad*	w.r.t. mech. ref.
pointing stability	≤ 50	*µrad*	w.r.t. mech. ref.
beam divergence[1]	50 ± 10	*µrad*	$\frac{1}{e^2}$ width
beam shape	Gaussian	–	–

and deformations of these components. Extensive testing for reliability of the most critical parts, i.e. the laser diodes, Pockels cell and polarizing beam splitter coating were done in life time tests by the laser manufacturer. 300 million shots were demonstrated in these life time tests and 500 million shots with the laser diodes alone. An effect of "infant mortality" of some laser diodes was observed during the first 20 million shots resulting in ~10% reduced output energy. However, mitigation of this was amongst others done by a burn-in of the laser diodes before integration to the FM [6], [7].

3. Transmitter verification

All handling and verification actions for the BELA transmitter were done in cleanroom class 100 (ISO 5) to avoid critical contamination. After basic electrical and functional tests of the transmitter to check the status of LHB and LEU, it was mounted to the optical test bench and optical performance measurements were done in atmosphere for reference. After this the transmitter was dismounted from the test bench and mounted into the thermal vacuum (TV) chamber. Using a red continuous wave (cw) laser the test adapter, on which the LHB was fixed, was aligned such that the optical axes of the transmitter and the optical setup are parallel. Then the performance of the transmitter was measured in the TV chamber. The transmitter Engineering Qualification Model (EQM) verification campaign took place March 1, 2013 to April 23, 2013 with some interruptions and the Flight Model (FM) campaign March 20, 2014 to April 8, 2014 (see Fig. 3).

3.1. Operations

In order to get a complete data set and to allow cross checking, telemetry (TM) data (housekeepings, science) from the application software (APS) (installed on the Digital Processing Module (DPM)) were recorded in addition to the external measured beam parameters. For time synchronization the BELA Quick-Look software used the system time of the operating system it was running on. Therefore the received TM packets during the tests are synchronized with that time and clear correlation is possible, which was useful for anomaly analysis and evaluation. The Mercury Interface Simulator (MIS) representing the interface to the S/C is used to command and monitor the transmitter. The MIS consists of a workstation (Windows PC), SFE, PFE and the corresponding SW (CMDVS, TSC, DB) (Fig. 4). Prepared test scripts included the commanding via telecommands (TC) to the APS on the DPM and were executed with the TSC. For live viewing (monitoring) and offline analysis (archiving) of the received TM packets during the tests the BELA Quick-Look SW was used. For coding of the TC and decoding of the TM packets the BELA database was used. All received TM data have been archived for later evaluation.

The LHB houses 2 complete lasers, main and redundant, which are built in cold redundancy. The LEU has 2 power supplies accordingly. Both lasers can be commanded by the main and redundant DPM in the ELU by cross-linked cable connections. This redundancy scheme shall ensure high reliability of the instrument. Performance and function were tested for the main and the redundant laser also using the cross-linked configurations.

[1] The beam divergence value is partly driven by the speckle noise caused by laser speckles. The speckle noise was optimized by adjustment of the beam divergence. This is explained in detail in Ref. [8].

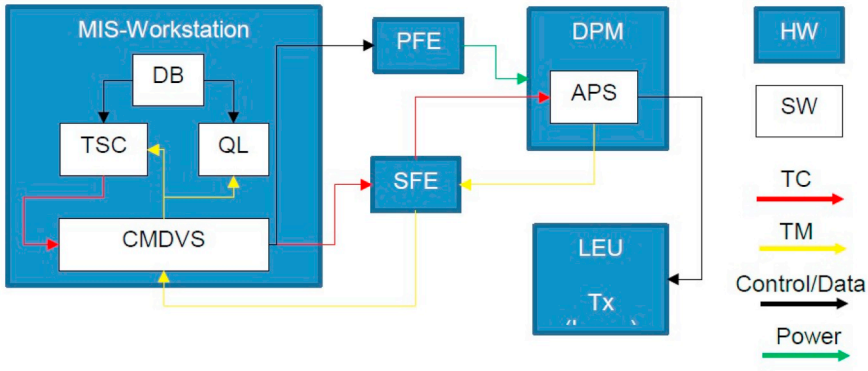

Fig. 4. Scheme of the Mercury Interface Simulator (MIS) acting as Electrical Ground Support Equipment (EGSE) used for commanding the ELU and the transmitter. Power is provided via the Power Front End (PFE) and the Power Converter Module (PCM) in the ELU to the LEU and telecommands (TC) and data packages are exchanged via the Spacewire Front End (SFE) to the Digital Processing Module (DPM). The Control, Monitoring, Data Processing and Visualisation Software (CMDVS) provides the I/F for the user.

Table 2
Qualification and acceptance temperature levels for the BELA transmitter.

model	min. non-operating temperature $T_{nop,min}$	max. non-operating temperature $T_{nop,max}$	min. operating temperature $T_{op,min}$	max. operating temperature $T_{op,max}$
EQM LHB	− 53°C	+ 73°C	− 8°C	+ 58°C
FM LHB	− 48°C	+ 68°C	+ 2°C	+ 38°C
EQM LEU	− 53°C	+ 73°C	− 33°C	+ 63°C
FM LEU	− 48°C	+ 68°C	− 28°C	+ 58°C

3.2. Thermal conditions

The EQM and FM transmitters underwent 8 and TV cycles respectively. These included maximum and minimum non-operating temperatures and operating temperatures. Performance testing was done within the operation temperatures including the applicable test margins and uncertainties. This means that test temperatures given in Table 2 were applied. For the last 2 cycles of the FM acceptance campaign the non-operational phases are not required. However, it has been decided to include a non-operational hot phase (during the 1st cycle) and a non-operational cold phase (during the 2nd cycle) in order to better investigate the performance and function of the transmitter, laser excluded to avoid stress. However, the laser underwent non-operational temperatures in previous tests. Thus, non-operational temperatures have been simulated for ELU and LEU, but not for the laser in order to avoid unnecessary stress.

These temperature values are applicable for the temperature reference point which is located at the LHB thermal strap and the LEU side and reflect the actual unit temperature. The Transmitter Baffle Unit (TBU) has a free optical aperture of 95 mm. This is the entrance for thermal radiation from the sun and from the hot Mercury surface. The TBU has a Stavroudis [9] shape to reject most of the incident environmental fluxes. It rejects about 70%. The remaining 30% are further reduced by the bandpass filter inside the TBU. This has a transmittance of 5.6% with regard to the sun spectrum. The baffle of the TBU reaches temperatures between −6 and +213 °C and in particular the front ring can reach up to +300 °C. The bandpass filter is in the range between −11 and 140 °C. However the flux onto the beam expander (BEX) collimation lens is never higher than 0.1 W which is necessary to limit the thermal impact on the LHB during orbit around Mercury. The resulting 0.73 K temperature difference across the filter is lower than the allowable 1 K and keeps thermo-elastic stress and opto-mechanical deformation low.

To verify that the transmitter baffle can survive the hot environment at Mercury a hot plate with high IR emissivity ($\varepsilon_{IR} > 0.9$) (temperature controlled up to 350 °C) was placed in front of the aperture. Although temperatures on Mercury range from -190-430 °C, controlled temperature was sufficient to simulate the correct heat flux onto the baffle [10]. By design the front ring of the baffle is able to withstand extreme temperature cycles. The yttria stabilized zirconia (ZrO_2) coating has a mixed crystal structure which has a good thermal cycling durability and reduces the heat transfer to the underlying substrate, in this case titanium grade 5 Ti6Al4V [11]. The thermal test showed that the transmitter works with specified performance in the operational temperature range and survives non-operational temperature without degradation.

3.3. Optical performance

The performance of the transmitter is in particular characterized by beam pointing accuracy, pointing stability and divergence. These determine how accurate the data output from the instrument can be and therefore need an intensive onground verification. For the verification during the dedicated campaigns an optical setup has been developed which is described in Section 4.4. Thermo-elastic deformations of the sapphire bandpass filter in the TBU were assessed according to the temperature distribution calculations. It was found that the temperature difference ΔT on the filter will be at maximum 0.7 K. If symmetrical on the filter this would cause only a change of laser beam divergence of about 1 μrad which is negligible whereas alignment would remain unaffected. However, from thermal analysis it was found that symmetry is not the case (Fig. 5) which is potentially critical for the alignment. Therefore the curvature of the filter surfaces due to temperature distribution was analytically calculated (Eqs. (1) and (2)) and a ZEMAX model was used to assess the beam deviation in dependence of the hot spot distance from the filter center. The result was that for the maximum distance of the hot spot from the center the beam deviation from the nominal alignment is 0.7 μrad. This is considered small enough to be neglected for the performance measurement in the thermal vacuum campaign. The introduced wavefront error is less than 0.01 waves and not significant. The radius of curvature R is calculated with

$$\Delta L = CTE_{Sapphire} \cdot \frac{t}{2} \cdot \Delta T = 1.13 \cdot 10^{-8} m \quad (1)$$

$$R = \frac{\Delta L}{2} + \frac{D^2}{8\Delta L} = 1.1 \cdot 10^{5} m \quad (2)$$

where t is the thickness of the filter and D is the diameter of the filter.

4. Testing campaigns

4.1. Vibration and thermal testing

The BELA transmitter EQM and FM first underwent vibration tests.

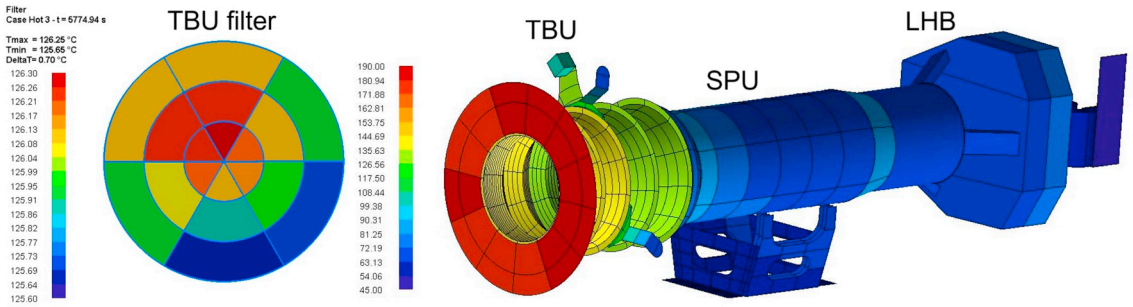

Fig. 5. Temperature distribution of TX for hot case in Mercury orbit.

These included sine search, full sine loads and full random loads in all three axes sequentially. Lowest Eigenfrequency for the LHB was found to be 275 Hz which is above the required 200 Hz. No structural failure was observed during and after testing. Eigenfrequencies remained constant before and after full loads vibration. All the vibration tests were done using bagging with a double folded protective plastic foil to keep contamination level low at 300 A/3 (i.e. particulate area coverage of 329mm^2 m^{-2} and molecular contamination layer of 330 ngcm^{-2}) [12]. A detailed visual inspection afterward in cleanroom class 100 (ISO 5) did not reveal any damage.

After vibration testing the transmitter, i.e. LEU together with LHB, was verified in a TV chamber within the qualification and acceptance temperature ranges. The temperature levels are shown in Table 2. As mentioned before, for the laser FM the design temperature was reduced to 5–35 °C range. This allowed the use of a thinner thermal strap at the FM LHB. Since the FM transmitter was primarily tested for performance and to limit the stress on the LHB unit, the temperature used in the test were only from 2 to 38 °C including only uncertainties of 3 K. Acceptance testing was done in a previous campaign at the laser manufacturer and is not discussed here. The EQM underwent 8 complete TV cycles at qualification levels and the FM 4 cycles at acceptance levels.

4.2. Transmitter setup integration

The units of the BELA transmitter (LHB, LEU) and ELU, necessary for control, were, after visual inspections and functional checks, integrated on their dedicated adapter plates onto the optical table inside the Space Environment Simulation Facility for Laser and Optic Experiments, namely SESiLOX, at DLR Adlershof laboratory. The FM LHB was mounted in vertical position, i.e. such that the laser beam exited in vertical direction. This was done because during EQM LHB verification it was found that gravity has a significant impact on bending of the bipods and therefore also beam alignment stability. It accounted to about 250 μrad or more which is over the required 50 μrad. Thus, the beam was folded with a 45° mirror above the LHB and out of the TV chamber through an AR coated window.

SPU and TBU were excluded in this test as they do not significantly influence the test. However, both units were tested separately, including the simulation of the hot Mercury surface.

The optical table was pulled out of the TV chamber to have a good accessibility to the units for these integration tasks and to connect all harness. Electrical grounding was realized with braided copper straps from the adapter plates to the units and to the TV chamber (Fig. 6). The required electrical grounding was verified by measurement with a calibrated multimeter. The harness from the LHB connecting to the LEU that provides the 100 A laser diode pump current is shielded with Kynar. This material has excellent electrical properties and is robust against environmental conditions. However it is rather stiff and needs a preforming before connecting between the unit in order not to degrade the alignment. For this reason the LEU is mounted sideways in the TV chamber setup. Preforming was done carefully using a hot air gun and tightly clamping the cable over a short distance when forming.

4.3. Functional testing

The transmitter units and ELU were tested at ambient, hot and cold temperature levels in non-operational and operational modes. The commanding and monitoring was done with the Mercury Interface Simulator (MIS) device (Fig. 4). This device, basically a 28 V power supply and a spacewire interface with a PC, simulated the interface to the spacecraft. All scripts necessary to operate the instrument were tested, both with and without the laser firing. Acquired housekeeping data (temperatures, voltages, energy data etc.) were compared and verified with external measurement data.

4.4. Optical testing

For characterization of the transmitter laser beam properties an optical setup has been developed. It was integrated onto an optical bench in front of the TV chamber where the transmitter tests were conducted. A 40-mm-thick optical window made of Corning 7980 fused silica provided the optical output of the chamber through a 240 mm clear aperture. An anti-reflection (AR) coating optimized for 640 nm and 1064 nm ensured low loss and limited back reflections which could either damage the laser itself or degrade the measurement signal. Despite the AR coating no additional mean to reduce back reflection or scattering was applied. The sensitive APD receiver part of the instrument was not part of this test. For such a test, i.e. in the total instrument configuration, an extremely high attenuation of about 160 dB is necessary [13].

The measurement of beam properties beam size, wavelength and pulse energy are rather straightforward. A schematic of the optical setup is shown in Fig. 7. Despite, measuring the angular pointing stability is the more challenging part because of its low magnitude. Therefore it was decided to use an off-axis parabolic mirror (OAP) with a large focal length of about 4000 mm. This increases sensitivity for the movement of the beam centroid on the camera, i.e. for the angular pointing. As large sensitivity means also sensitivity to errors, a second laser was introduced in the setup to provide a reference. Then by comparison of the reference laser and the BELA transmitter laser errors can be compensated out. The rule of thumb for the achievable angular pointing accuracy with a CCD based camera is approximately one tenth of a pixel. Thus the theoretical accuracy of the camera used here is below 1 μm [14]. As the principle of measurement relies on relative positions of the beam centroids, the exact knowledge of the pointing of the reference mirror, representing the mounting plane of the LHB, is not required. But it is very important that the reference mirror does not move relative to the mounting plane. The reference mirror is mounted within 100 μrad with regard to the laser beam. But the laser beam must be coaxial with the optical axis of the measurement setup, i.e. the OAP. Different techniques to achieve this are available, e.g. auto-collimators or interferometers. Another option is using marks on the edges of the OAP. First are rather complex and latter is in general accompanied with a large alignment error. In order to find the optical axis and the focal point of the OAP in a reasonable accurate way a procedure where a pair

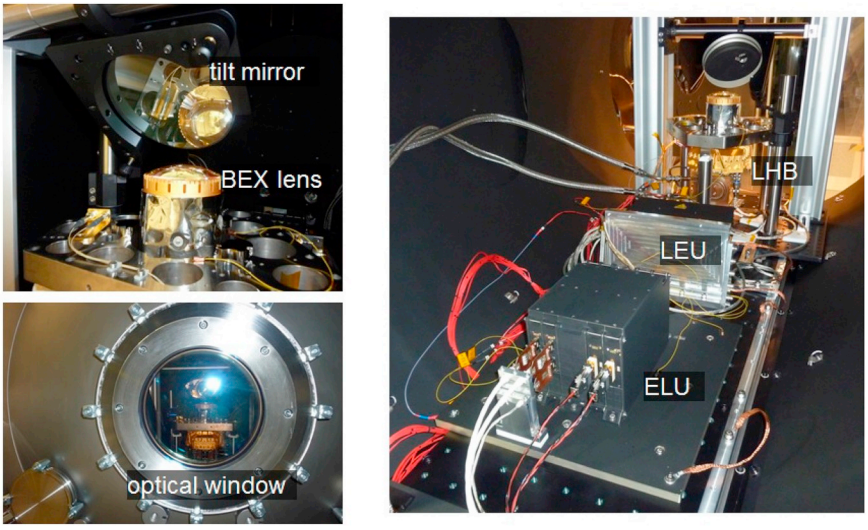

Fig. 6. BELA transmitter and ELU setup in the TV chamber at DLR Adlershof. The upper left image shows the LHB pointing upwards below the fold mirror to redirect the laser beam through the TV chamber optical window. On the right the complete setup with the electronic boxes can be seen.

of parallel laser beams illuminating the OAP aperture was used as described in Ref. [15]. A mirror at the intersection point of the two laser beams is used to direct the light of one of the laser beams back to the OAP out of plane to the other two beams. Then the OAP is adjusted such that the third laser beam is parallel to the other two. Finished with this the optical axis of the OAP and the focal point position are known. Though this is a simple and straightforward procedure without usage of complex devices, it is sufficient for the measurement task. Achieved accuracy is about 3 mrad and thus introduces no significant image aberrations (see Fig. 8).

A matter of fact is that the pointing stability of the reference laser is not ideal. This also translates into the signal for the reference laser beam spot. But this proportion is not included in the BELA transmitter beam spot. Therefore it adds an error to the measurement. As this effect cannot be wiped out, a very stable reference laser is used to keep the effect small. Additionally, the laser beam of the reference laser passes a beam expander with magnification factor of 20, which improves the pointing stability by a factor of 20. Pretests with this reference laser showed that it has an angular stability of better than 1.3 μrad without BEX and about 0.07 μrad with BEX [16]. The temperature stability of the reference laser is better than 5 μrad K^{-1} [17]. The temperature in the cleanroom was controlled to about 22°C. Therefore the error of the reference laser is negligible.

The high dynamic range of the laser beams intensity were adjusted

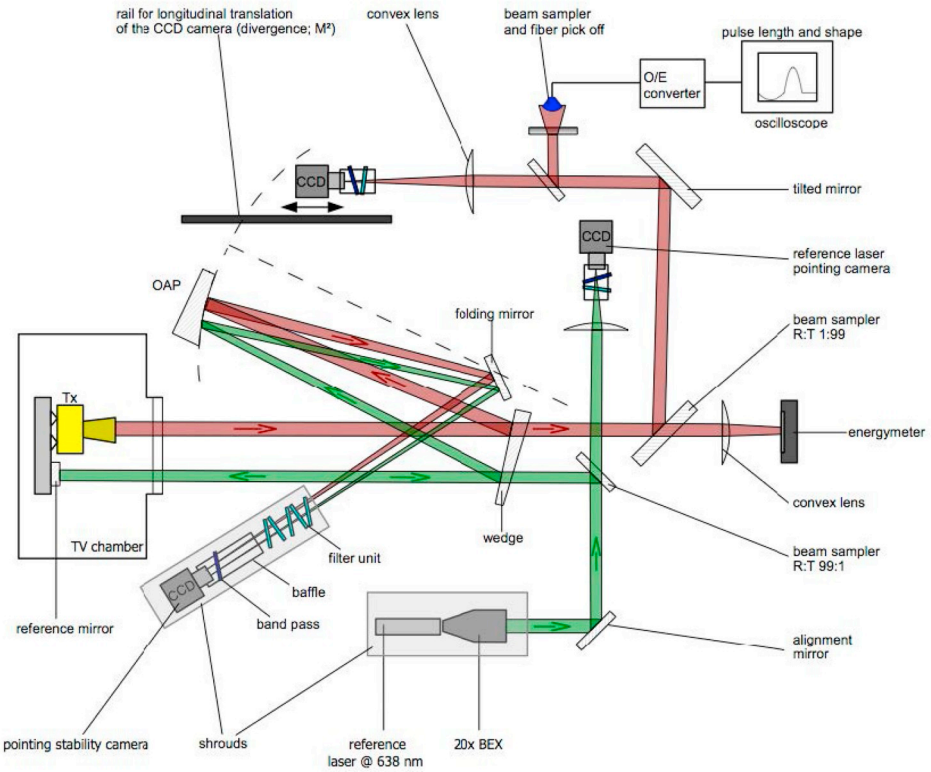

Fig. 7. Schematic of the optical bench setup equipment.

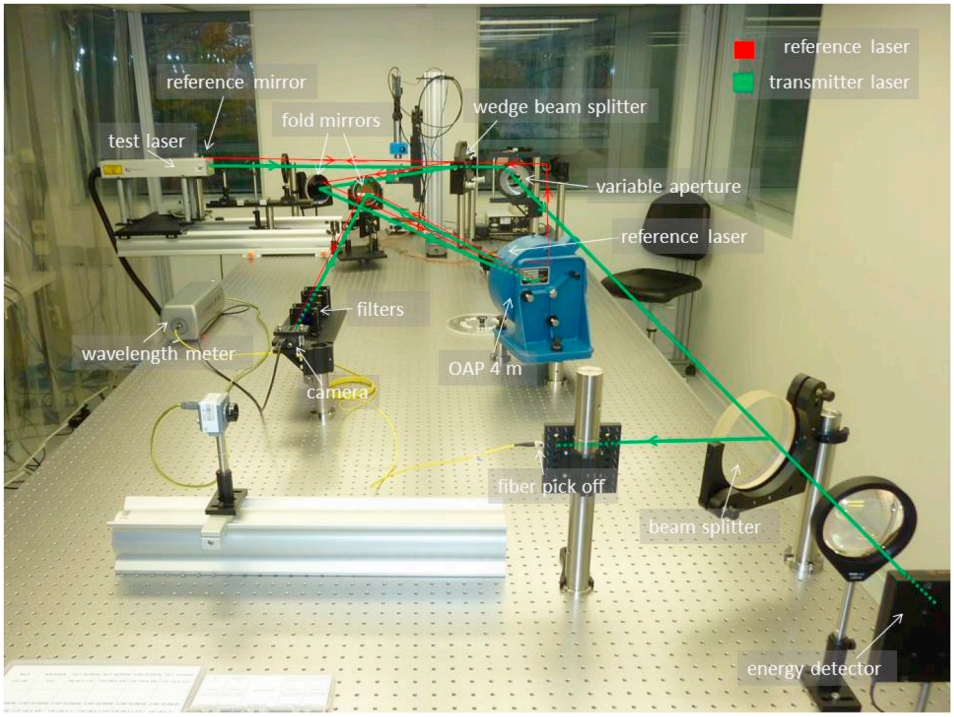

Fig. 8. Optical setup in cleanroom class 100 (ISO 5) for measurement of the transmitter laser beam parameters during thermal vacuum tests. Here for test purposes a test laser with similar beam parameters like the BELA transmitter is used.

with an optical filter unit. The laser beam of the BELA transmitter has a diameter of about 74 mm, 5.5 ns pulse width and the pulse energy is 50 mJ (equivalent to approx. 10 MW peak power). The reference laser is a continuous wave laser at a visible wavelength of 638 nm and has merely a continuous power of about 50 mW and a not expanded diameter of about 1 mm. The difference in intensities respectively in power between the BELA laser and the reference laser is large, in numbers about 160 dB. This means a detector must have a either a huge dynamic range or the beams must be balanced properly. As most CCDs have a dynamic range of about 60 dB, the beams were balanced using wavelength dependent filters that attenuate the two beams differently. The used filters were Schott KG and NG glasses. Schott KG as attenuator for near IR wavelength and transmissive for visible wavelengths.

Big disturbances in the optical components that could deflect the beams away from the camera area (a CCD with an area of about $7.1\,x\,5.4\text{mm}^2$) were mitigated using stable opto-mechanical components, active and passive damping of the optical tables, temperature control and shrouds for single units. A baffle between TV chamber and optical table limiting air turbulence was used also. In order to reduce vibrations introduced by the vacuum pumps, cooling units or by the floor itself the TV chamber is air damped. The time was synchronized between Mercury S/C interface simulator (MIS) and measurement setup to correlate system internal H/K data and external measurement data.

The reference laser moves double the value of what the BELA transmitter moves when the baseplate moves, and is considered in Eqs. (3) and (4)). The geometric relations are depicted in Fig. 9.

$$\vec{\delta} = \vec{\eta_0} - \vec{\xi_0} \tag{3}$$

$$\vec{\Delta} = \frac{\vec{\eta_0}' - \vec{\eta_0}}{2} - \vec{\delta} \tag{4}$$

Herein $\vec{\delta}$ is the initial centroid position offset, $\vec{\eta_0}$ and $\vec{\xi_0}$ are the initial centroid positions and $\vec{\eta}'$ and $\vec{\xi}'$ the current ones. $\vec{\Delta}$ is the relative shift of the BELA transmitter spot centroid on the camera plane in the focal plane of the OAP. The relative angular movement of the transmitter laser beam is then calculated using

$$\vec{\alpha} = \frac{\vec{\Delta}}{f} \tag{5}$$

with f being the focal length of the OAP and with

$$\vec{\alpha} = \begin{pmatrix} \alpha_x \\ \alpha_y \end{pmatrix} \tag{6}$$

being the angular deviation vector.

4.5. Measurement of start pulse fiber output

There are two optical fibers coming from the LHB for start pulse detection. They pick off a small proportion (about 4 to 8 fJ) of the exiting laser light from the BEX and direct it to the APD. The signal must be within certain limits, sufficient for reliable start time determination and not too high to saturate the detector or even to destroy the fast transimpedance amplifier which is in particular susceptible for very short pulses. Therefore careful adjustment of this energy proportion was performed via insertion of a pinhole at the fibers.

During firing the laser without the SPU and TBU integrated a ring around the central spot was seen in the near field, having a diameter of about 0.4 *m* at a wall in 4.5 m distance. This is a typical feature of the unstable resonator with a graded reflectivity profile outcoupling mirror. In the far field this profile propagates to a Gaussian shaped profile with diffraction rings. Although this ring contains only a small fraction of energy there was concern that it eventually is back-reflected at parts of SPU or TBU and then fed into the fiber pick-off. Thus, this portion of energy needs to be regarded as a straylight source which has the potential of damaging the receiver's detector. The critical threshold, i.e. the maximum rating of the APD, is 50 mW incident radiant flux within 30 ns. A measurement of the start pulse fiber output while varying the distance of a screen in front of the laser showed, that a change of pulse energy at the end of the fiber was detectable. But the change was on the order of 10 … 20%, i.e. on the order of the required output for reliable

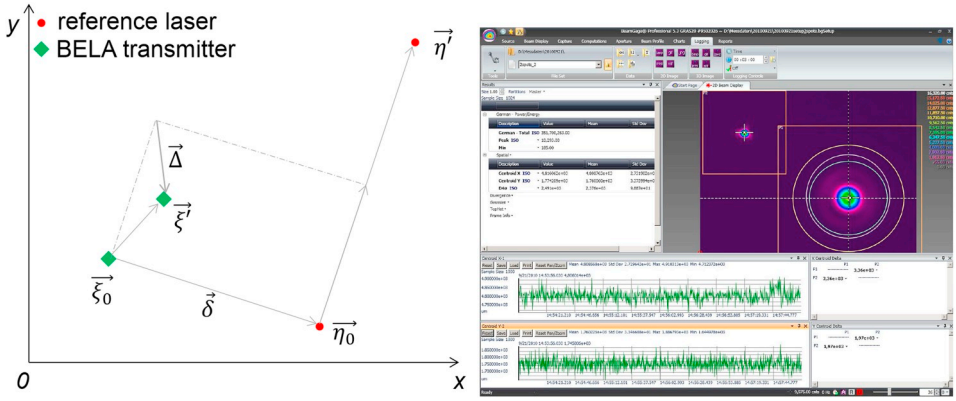

Fig. 9. Left: Sketch of the geometric relations for the positions of reference laser and BELA transmitter centroid positions. Right: Screenshot of two laser spots using the Ophir BeamGage beam analysis software, accessed via a LabView interface.

start pulse detection.[2] Therefore the risk for a damage of the APD in the receiver was regarded negligible. However, the risk of damaging the APD is only given in a laboratory environment where close objects in the beam path could scatter light into the receiver. In flight operation configuration this is not an issue.

4.6. Testing with integrated SPU and TBU

For verification that the SPU and in particular the TBU with the optical filter have no significant influence on the pulse energy and the beam profile measurements with and without these units were performed. The direct measurement of the energy ~0.3 m away from the LHB yielded about 53.7 mJ (at 21 °C) for the main laser. When integrating the TBU in between the LHB and energy detector no change could be observed. Also in a test were a filter substrate as used in the TBU was put between LHB and energy detector no pulse energy change could be observed. The transmission of the filter substrate including optical coating is 0.995 which corresponds to 0.25 mJ. Concerning also a fluctuation range of about ± 1.5 mJ for the main laser the attenuation of the optical filter is not measurable. Therefore it can be concluded that these units (SPU and TBU) do not impact the beam significantly. The maximum irradiance in the vicinity of the integrated laser was measured with a level of $7{\cdot}10^{-8}$J m^{-2} directly in front of the TBU aperture with the beam dump attached. Hence, SPU is light tight.

5. Test results and discussion

In this section the measurement results obtained in the test campaigns for EQM and FM are presented. For overview not the complete data are shown but significant aspects are pointed out. Fig. 10 shows an overview of when the performance tests where performed for the FM.

5.1. Energy measurements

Test results are summarized in Tables 3 and 4 at the end. Pulse energy is slightly below 50 mJ in some cases. This is a minor and acceptable deviation considering measurement accuracy of 3% (1.5 mJ) of the energy detector. However, there are reserves in the laser which ensure to keep the energy constant at these levels till EOL. Fig. 11 shows the starting and stabilization phases of the laser operation. Pointed out are also in detail the first seconds which show the performance of the energy control loop. A warming up effect can be seen in the curves.

[2] The pulse energy of the outgoing pulse is measured with an internal energy monitor inside the LHB. This is calibrated to 5% accuracy and is compliant with science requirements of relative shot-to-shot accuracy of 5% and absolute reflectivity measurements to within 20%.

5.2. Energy measurements over temperature change

The effect of temperature variation on the laser energy is pronounced for the EQM, but the effect is minimal for the FM laser as shown in Figs. 12 and 13. This is due to a better calibration of the energy monitor and control loop for the FM. Only a warming up effect is observed here, which is expected.

5.3. Overview energy measurements

The comparison of pulse energies shows a quite wide spread for the EQM at different temperatures. It ranges from about 45 mJ to about 55 mJ for the main laser (m). The EQM redundant laser (r) shows a similar behavior, though at a lower pulse energy level (Fig. 13).

The FM lasers show a more stable behavior. The pulse energies for main and redundant laser are at 50 mJ or slightly above. The difference between cold, ambient and hot temperatures are much smaller in the range of 4 mJ. Worth mentioning is that the main laser performs even better than the redundant laser in terms of constant energy.

5.4. Wavelength measurements

The wavelength of the emitted light of a Nd:YAG rod shifts with temperature. Fig. 14 shows the wavelength in vacuum at different temperature levels. The change of wavelength is within the specified range. The higher variation for EQM is explained by the higher and lower temperatures applied to the units (Table 2).

5.5. Overview wavelength measurements

Fig. 13 shows on the right the overall measured wavelengths for different models. With increasing temperature the wavelength increases as well by about 5 pm K^{-1}, but remains as stated before within the acceptable range.

5.6. Housekeeping pulse energy vs. external measurement

Table 3 shows the laser pulse energies measured externally, the internally measured H/K energies (energy AS, after shot) and the pump pulse widths. The latter are a measure for the energy pumped into the laser rod. One can see that pump pulse width is rather similar for main and redundant laser but varies with temperature. This is due to the fact that the pump diodes shift their wavelength with temperature by about 0.2 nm K^{-1}. This means that there is an optimal temperature for best absorption and therefore best efficiency in the Nd:YAG laser rod. It can be seen that the redundant laser is slightly more energy efficient at lower temperatures, whereas the main laser performs better at ambient and hot temperature. This is probably due to slight differences in the

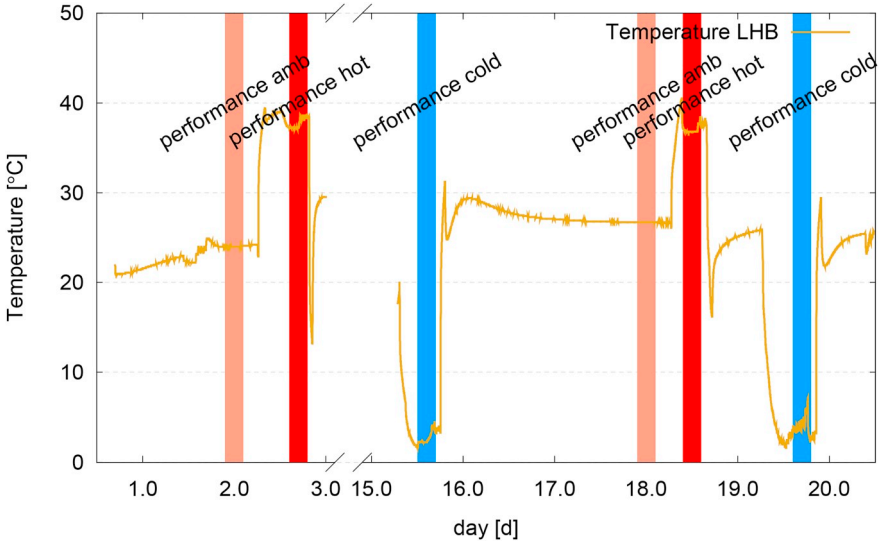

Fig. 10. The temperature curves for the LHB with indication of performance tests are shown.

Table 3
Summary of the measured pulse energies for the FM transmitter with the pump durations included. Ext. energy is the externally measured pulse energy, energy AS (after shot) is the H/K, i.e. internally measured energy and pump pulse width the duration, i.e. a measure for the pump energy into the laser rod. Herein M-M, M-R, R-M, R-R denote the operation configurations (cf. Fig. 12).

		M-M		M-R		R-R		R-M	
		10 Hz	1 Hz	10 Hz	1 Hz	10 Hz	1 Hz	10 Hz	1 Hz
amb	ext. energy [mJ]	51.7	48.9	54.6	53.8	50.0	49.9	50.3	47.9
	energy AS [mJ]	50.1	49.8	49.9	49.9	50.2	49.8	50.2	48.9
	pump pulse width [μs]	117.5	117.5	125.0	125.0	112.5	115.0	112.5	115.0
hot	ext. energy [mJ]	50.0	47.5	51.0	50.0	50.1	49.6	47.9	50.9
	energy AS [mJ]	50.1	49.7	50.1	49.9	52.2	49.9	49.8	49.4
	pump pulse width [μs]	87.5	85.0	90.0	92.5	87.5	90.0	82.5	87.5
cold	ext. energy [mJ]	47.1	47.2	52.4	52.3	48.4	49.1	49.3	49.2
	energy AS [mJ]	50.1	50.3	49.9	50.5	50.2	50.7	49.7	50.6
	pump pulse width [μs]	92.5	92.5	87.5	82.5	82.5	80.0	95.0	95.0

Table 4
Summary of most relevant measured values. Columns “M” and “R” are for the main and the redundant laser.

parameter	f [Hz]	ambient case		hot case $T_{op,max}$		cold case $T_{op,min}$		comment
		M	R	M	R	M	R	
divergence [μrad]	1	60 ± 6	56 ± 6	53 ± 4	53 ± 4	59 ± 4	45 ± 4	
	10	60 ± 6	56 ± 6	60 ± 4	57 ± 4	57 ± 4	52 ± 4	
pulse energy [mJ]	1	49.0 ± 0.5	50.0 ± 0.6	50.8 ± 0.6	50.2 ± 0.7	49.2 ± 0.6	49.2 ± 0.6	
	10	50.3 ± 0.5	50.0 ± 0.5	50.3 ± 0.6	50.3 ± 0.4	50.3 ± 0.4	52.3 ± 0.5	
pulse length FWHM [ns] width at 10% [ns]	1	5.3 ± 0.2 14.3 ± 1.	6.0 ± 0.2 15.7 ± 1.6	5.5 ± 0.2 15.1 ± 1.5	7.2 ± 0.2 19.2 ± 2.0	5.5 ± 0.2 14.1 ± 1.5	5.8 ± 0.2 15.0 ± 1.5	
	10	5.1 ± 0.2 14.4 ± 1.5	7.7 ± 0.2 20.0 ± 2.0	5.7 ± 0.2 15.4 ± 1.5	7.6 ± 0.2 19.9 ± 2.0	5.5 ± 0.2 14.1 ± 1.5	6.6 ± 0.2 16.7 ± 1.7	
pointing deviations over temperature [μrad]	10	–	–	21 ± 11	53 ± 8	0	0	cold case is reference
pointing deviations over time [μrad]	10	–	–	< 9.0	< 9.0	< 10.6	< 11.3	
wavelength [nm]	10	1064.483 ± 0.004	1064.479 ± 0.004	1064.558 ± 0.004	1064.559 ± 0.003	1064.371 ± 0.005	1064.352 ± 0.001	

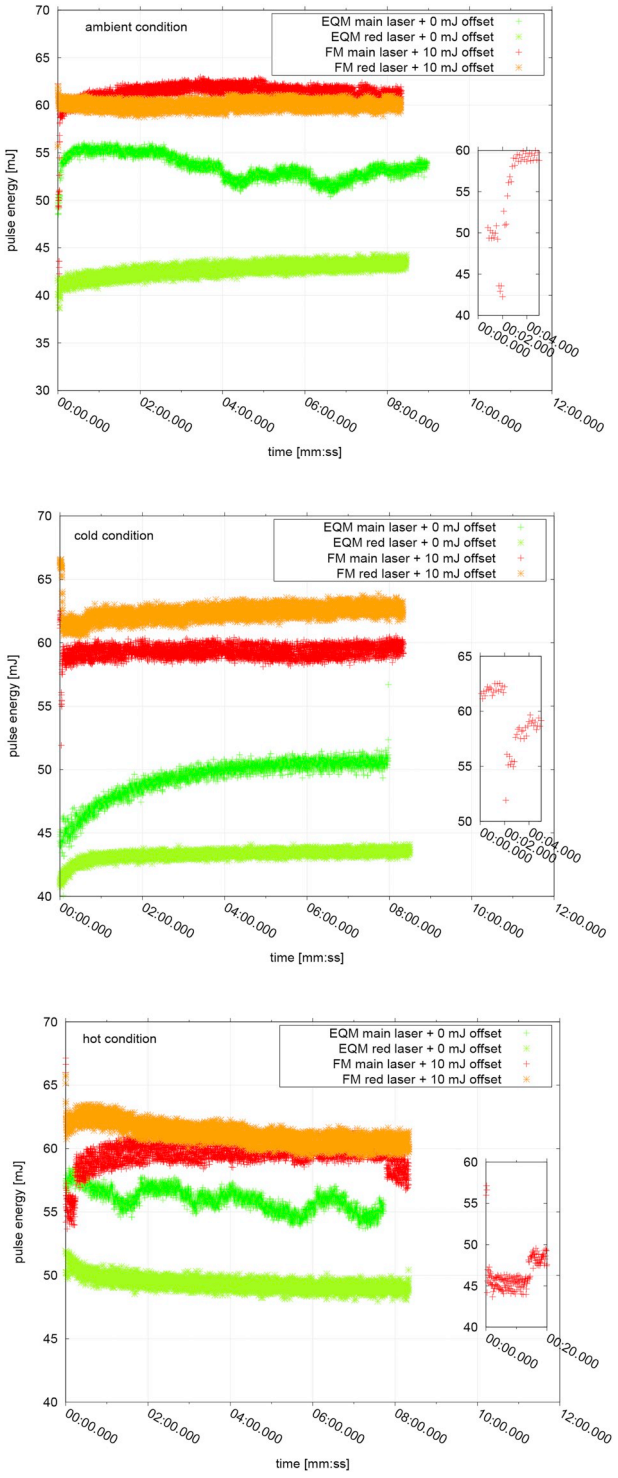

Fig. 11. Pulse energy of the EQM and FM in ambient, cold and hot temperature conditions. Fluctuations and warming up effects can be seen in particular for the EQM laser.

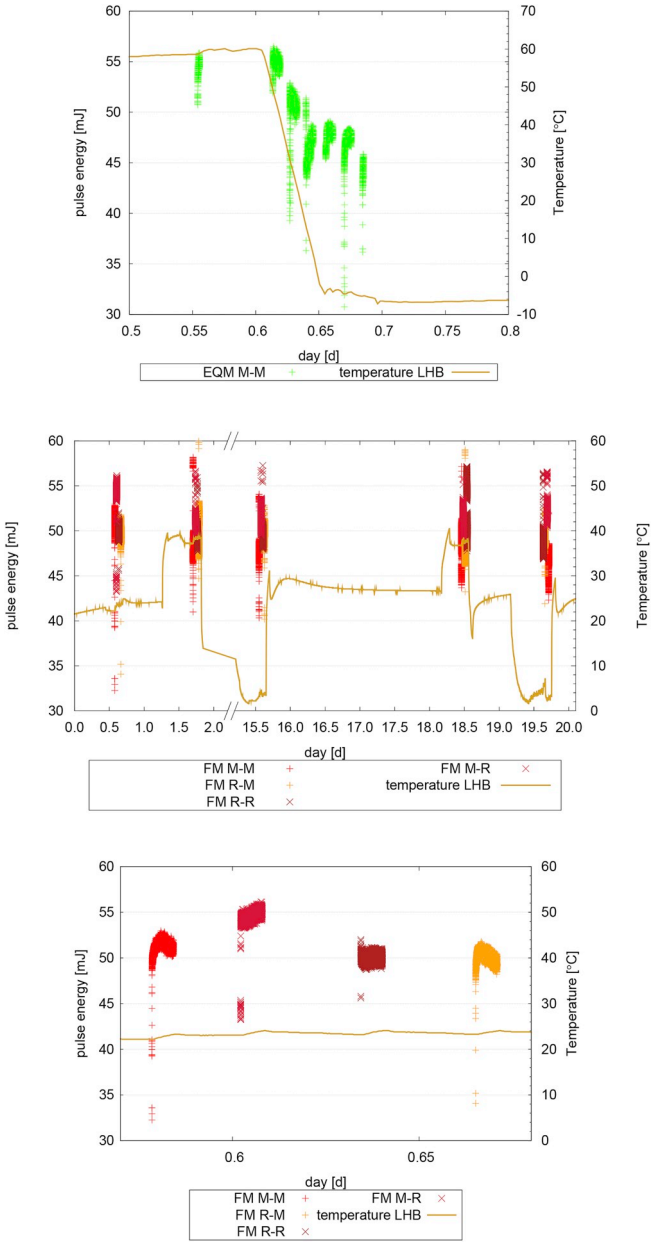

Fig. 12. These plots show pulse energy dependence on the temperature. On top the EQM behavior is depicted. The middle and bottom graphs show the FM behavior overview and detail at ambient temperature. Herein M-M, M-R, R-M, R-R denote the operation configurations, i.e. M-M means that the main DPM and PCM in the ELU operate the main laser in the LHB. Other combinations are analog.

laser cavity alignment and due to a different spectrum, i.e. central wavelength (808.4 … 809.5 nm) and spectral width (2.2 … 3.5 nm), of the pump diodes. Keeping the laser diodes in a certain tight temperature range would require an active temperature control attached directly to them. With the passive temperature control via thermal strap at the backside of the LHB this is not possible. However the length of the laser diodes pump pulse width is in the order of 80–100 µs This is about 40% of the maximum pump pulse width that can be set and leaves the laser enough reserves to fulfill the pulse energy requirements over the complete operating temperature range. Fig. 15 shows the behavior over time.

5.7. Spatial pulse profile

The spatial pulse profile was recorded in order to evaluate the beam quality and to determine the divergence. They can be calculated using the $1/e^2$ beam width and the focal length of the focusing element, i.e.

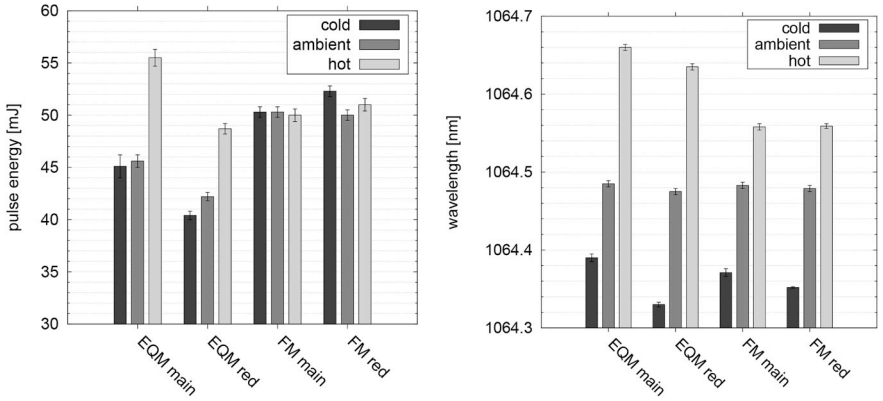

Fig. 13. Overview of measured pulse energies for different models and temperatures (left) and of measured wavelengths (right).

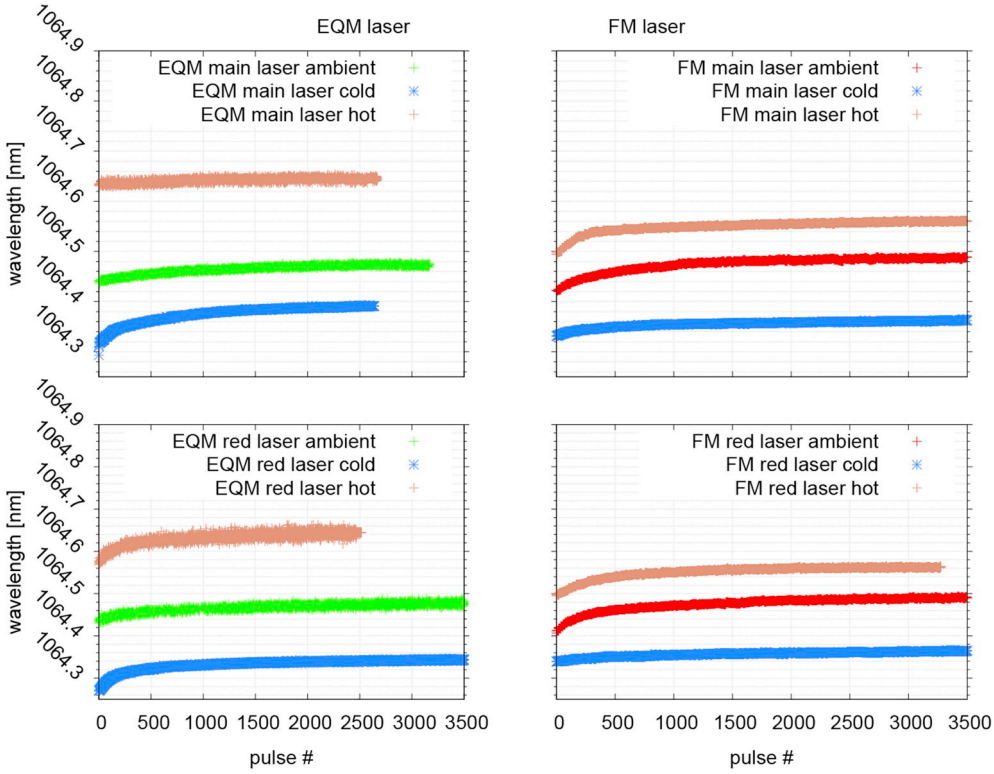

Fig. 14. Measured wavelength for EQM and FM at different temperature conditions.

the OAP in the measurement setup. The ideally focused laser beam diameter was calculated with 197.7 μm using the Gaussian beam equation and the determined M^2 value of about 2.7:

$$\tilde{D}_0 = M^2 \lambda \frac{4}{\pi} \frac{f}{D_0} \tag{7}$$

For a collimated laser beam following equation for the divergence is valid

$$\Theta = \frac{D_0}{f} \tag{8}$$

Herein $\tilde{D}_0$ is the focused beam diameter, λ is the wavelength, f is the focal length and Θ is the laser beam divergence angle. The measured beam diameters of about 200 μm to 250 μm give a divergence of the laser beam of about 50 μrad to 60 μrad. This is inline with the requirement. The used CCD camera has a square pixel size of 4.4 μm, i.e. the focused beam covers about 45 pixels. This is well sufficient for a reliable beam measurement [18]. Furthermore the spatial beam profile is an important influence factor for the inversion of the received signal to get information about the surface, e.g. slope, roughness and range [19] and [20]. Figs. 16 and 17 illustrate some representative spatial beam profiles in the far field. One can see that in general a good approximation to a Gaussian shape is achieved. The redundant laser has a more elliptical form, whereas the main laser has a slightly irregular shape with some energy in a side lobe. For both lasers it is obvious that in the cold case the profile is smallest and also closest to a circular and Gaussian

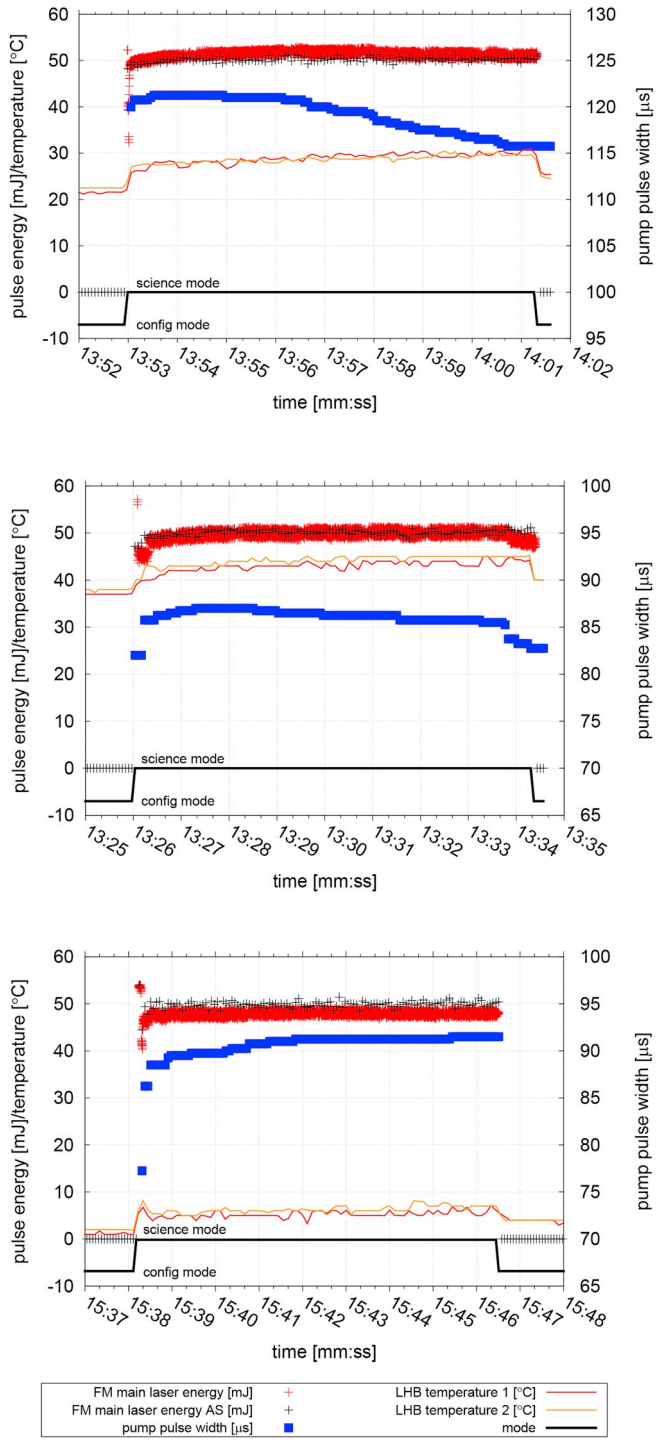

Fig. 15. Typical external (FM main laser energy) and housekeeping energy (FM main laser energy AS) measurement curves in dependence of the temperature.

shape. In general it must be remarked that these are snapshots of the beam profiles. There is some variation from shot to shot which depends on pump energy variations and cavity perturbations. The drift of the beam profiles with temperature is expected to result from small geometrical changes in the cavity. Contamination is not assumed to be responsible for this effect. The noticeable rotation of the major and minor axes for main and redundant laser might be due to different geometrical orientations of the two lasers in the LHB in combination with the beam combiner and temperature change. These are not considered critical as most of the energy is still within the beam width (86.5% within $40 - 60\,\mu$rad).

5.8. Temporal pulse profile

The temporal pulse shape and in particular the length of the laser pulse is an important parameter for the instrument's performance. Short pulses are required to achieve a good SNR. The following plots shows the temporal pulse shape of the FM main laser. It is very similar also for the redundant laser and the EQM lasers. It can be seen that the pulse profile is very close to Gaussian, as it is expected for a actively Q-switched laser. The width of the laser profile is about 5 *ns* (FWHM). This is in accordance with the required width of 2.5 to 8.0 *ns*. Also the width at 10% of peak is with about 15 *ns* below the requirement of less than 18 *ns*. Main and redundant laser have very similar pulse shapes. The redundant laser though had slightly wider pulses, i.e. 1.1 to 2.6 *ns* for the FWHM length longer depending on the ambient temperature conditions. This is inline with the requirements and thus acceptable. The pulse shapes where acquired with an 1 GHz bandwidth oscilloscope, but averaged over 128 pulses. For the not averaged shapes there where some fluctuations (mode beating) observable, which where due to the small resonator length quite moderate and not critical for LIDT (see Fig. 18).

5.9. Pointing stability

Fig. 19 shows the variation of the beam centroid position as detected on the CCD camera in the focus of the OAP. The position or change of position of the centroid is a direct measurement for the beam angular pointing. The angular pointing is simply calculated by

$$\alpha_{x,y} = \frac{\Delta_{x,y}}{f} \tag{9}$$

with $\alpha_{x,y}$ being the angular pointing in x or y direction, $\Delta_{x,y}$ the shift of the beam centroid on the CCD camera in x or y direction and f the focal length of the focusing element, i.e. the OAP. The stability of the optical setup itself was determined to be better than 10 μrad. The cold case is used as a reference here. Therefore they are settled at the 0 μrad, 0 μrad position. In the hot case both lasers have changed their direction with regard to the initial direction, the main laser by about 21 μrad and the redundant laser by about 53 μrad. These shifts are partly contributed to the laser optical bench itself and partly to the laser head box. A discrimination is not possible here. The required 50 μrad are exceeded slightly but it was considered acceptable.

The angular deviation of the laser beams of the laser beams for the TOP Max versus the TOP Min were compared. The deviation of the main laser is about 21 μrad ± 11 μrad. The deviation of the redundant laser is about 53 μrad ± 8 μrad. It must be noted at this point that the test was done on the baseplate dummy made from INVAR. This has a close to zero coefficient of thermal expansion (CTE) and represents the flight configuration with a zero CTE CFRP panel very well. Larger beam deviation than on the FM baseplate might be due to that fact. The time resolved pointing for different temperature levels is shown in Fig. 20.

6. Conclusions

The BELA EQM and FM transmitter lasers, i.e. LEU and LHB together, have been successfully verified and accepted for delivery to the University of Bern for integration into the BELA instrument. Significant lessons were learned concerning the hardware in the EQM test

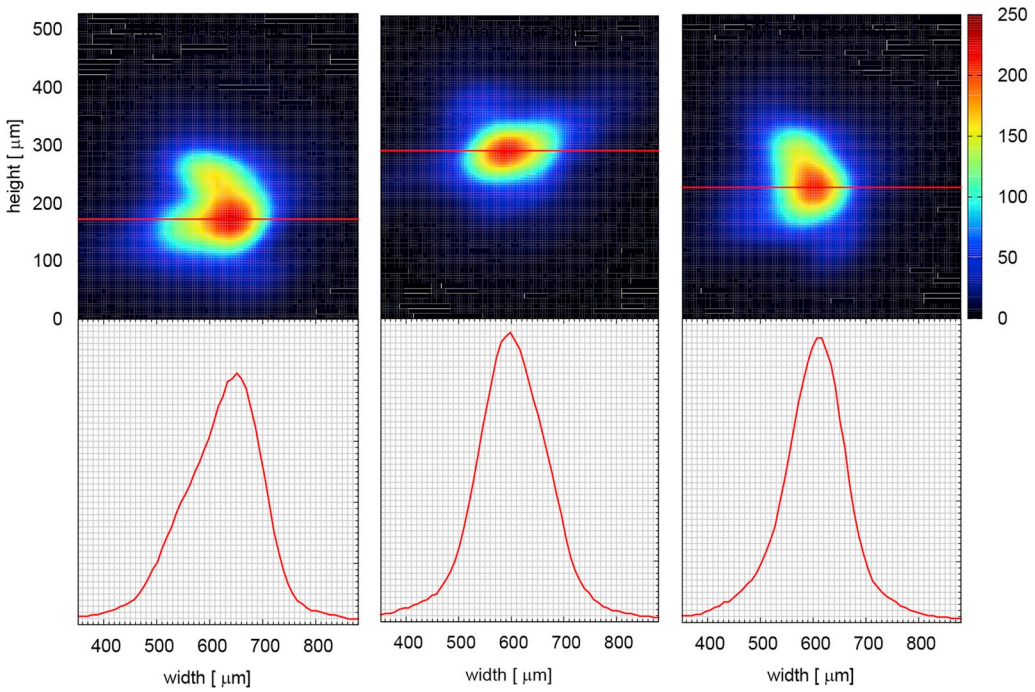

Fig. 16. The spatial beam profiles for the main laser in the far field are shown, i.e. shown is the focused spot of the beam on the camera. Left: ambient temperature, middle: cold case, right: hot case.

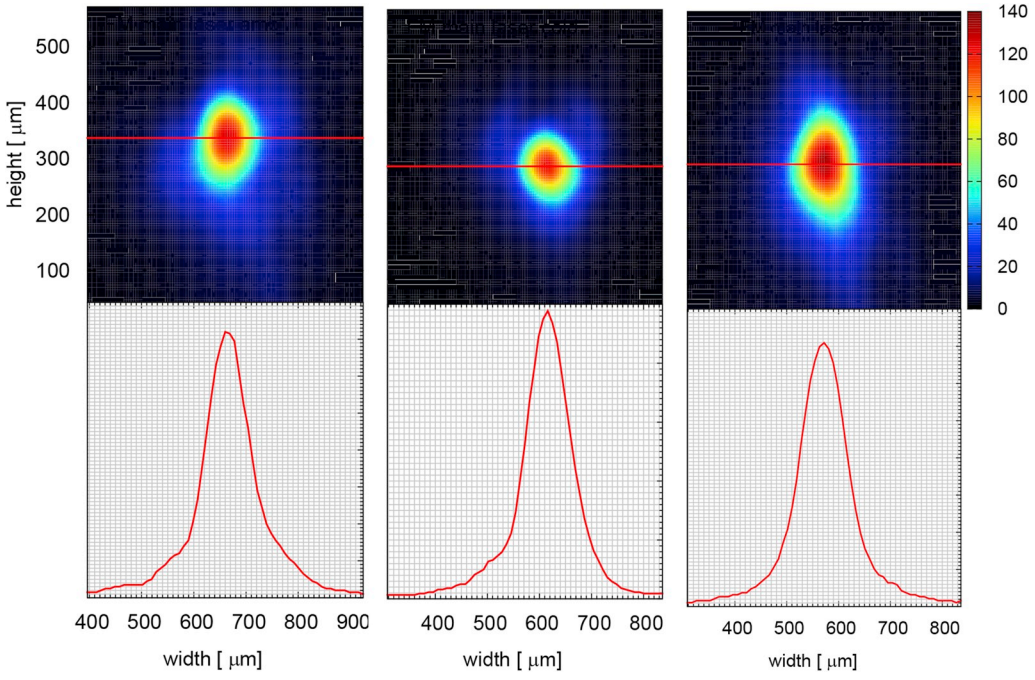

Fig. 17. The spatial beam profiles for the redundant laser in the far field are shown, i.e. shown is the focused spot of the beam on the camera. Left: ambient temperature, middle: cold case, right: hot case.

campaign in the first half of 2013, that were incorporated into the design of the FM. Testing of the FM was conducted in March and April 2014. EMC behavior was improved using a double shielded harness for the 100 A laser diode pump current. The negative effect of this pump current was also mitigated by implementation of a ramp load control for the laser pump diode, i.e. the $\frac{di}{dt}$ term for the capacitors was reduced meaning driving up the load current for the capacitors smoother. Failure tolerance, especially when switching instrument modes was improved and made more robust. In particular improvement was achieved for the acquisition of housekeeping data and reducing temperature dependence, in particular for the energy control loop. The energy monitor temperature dependence was reduced by reading the

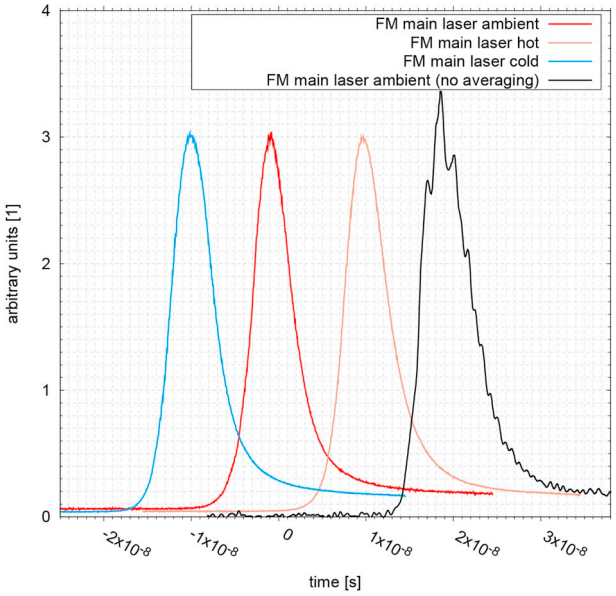

Fig. 18. Temporal pulse shape of the FM main laser at different temperature conditions. The pulses are offset by 10 ns on the time axis for better visualisation. The trailing edge is a effect of the finite rise time of the active Q-switch which reduces loss even 10 ns after the main pulse is emitted [21]. Except for the not averaged profile the shapes are averaged over 128 pulses and acquired with an oscilloscope of 1 GHz bandwidth.

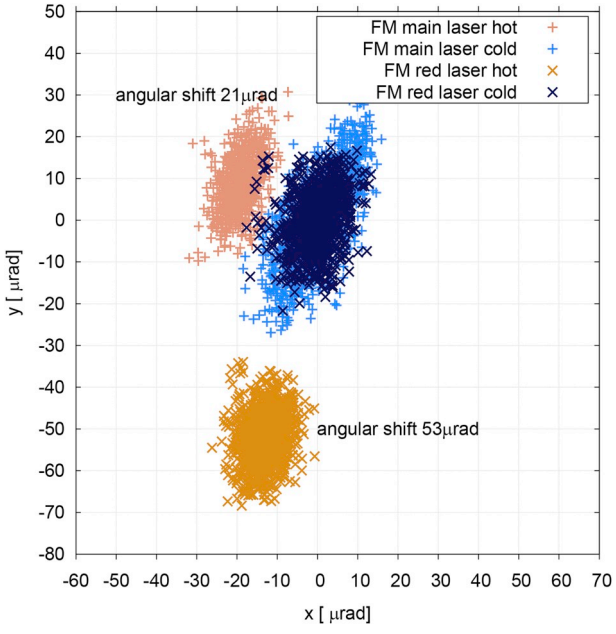

Fig. 19. Angular pointing stability for the FM main and redundant laser. A temperature related drift is clearly visible which is overlaid by a jitter.

internal pulse energy value just after the Pockels cell pulse. The remaining temperature dependence was compensated by the laser control module (LCM) software with measured temperature data giving a compensated energy monitor signal. This resulted in a more stable pulse energy output. Also the temperature dependence of the Pockels cell driver rise time was verified as being adequately compensated by the energy control. Much effort was invested in reducing this rise time in order to meet the required pulse energy output of 50 mJ at BOL. Finally, it was demonstrated that the FM laser is capable of generating up to 60 mJ pulses, which shows that there is some margin for the compensation of degradation effects in space during the mission by means of the energy control. The maximum settable pump pulse width is 250 μs (Table 3). A dedicated derating was done for the electronics to ensure lifetime. The laser diodes, which are operated nominally at 100 A, have even been tested without special issues at 150 A. The optical components and coatings where tested for LIDT and have factor 4 or higher of occurring energy densities in the resonator. Therefore it can be stated that the lasers inhabit sufficient margin even exceeding lifetime. It was found that the temperature calibration is essential for a stable and reliable pulse energy output. Unit operation anomalies were detected that were caused by temperature sensor noise and offsets for different operation modes, which led to unwanted interruptions of operations at the temperature extremes, especially in cold cases. These anomalies were investigated and successfully resolved. There was a dependency of the housekeeping temperature sensors (model AD590) on the operation modes of the instrument which was up to 10 K between science mode, configuration mode and standby mode. A compensation for this was implemented by changing calibration values for temperature acquisition depending on operational mode. Another lesson learned was not to join the electronics part in the LHB with the optical part in a common hermetically sealed compartment, but rather to separate it for easier repair or refurbishments.

There was also improvement of the measurement setup used for the campaign. The influence of gravity on the transmitter on alignment and pointing stability during temperature cycling testing on-ground was minimized by the change to vertical position of the transmitter and is considered as mandatory for achieving meaningful measurements. Careful encapsulating of the beam path and the optical setup reduced air turbulence and pointing measurement error. Further it was demonstrated that a real time measurement of beam pointing stability with high accuracy, of the order of 5 μrad is possible at DLR facilities with the setup described. The developed data acquisition system, which gathers all relevant optical data and provides real-time statistics, provided an instant overview of the transmitter status. The robustness of the transmitter against the hot Mercury environment up to 320°C has been verified meaning the implemented provisions of heat input reduction work and limit the warming of the system. The verification campaign demonstrated that the transmitter met all the performance and functionality specifications of the BELA instrument. There is sufficient margin to compensate for degradation effects during the long cruise phase and scientific data acquisition is ensured. Robustness to random vibration loads and shock was verified. Settling effects are minimized by workmanship shaker tests. Hence, the test campaign at unit level ensured the delivery of a correctly working BELA transmitter prepared for the integration in the BELA instrument.

Acknowledgements

This was possible because of the effort of all involved team members. Many thanks go to all involved collaborators in the BELA transmitter team and the co-authors who contributed for the successful delivery of the instrument. Further we thank the anonymous reviewers and the editors for their constructive comments which greatly improved the manuscript. Financial support was provided undergrant 50QW0501 on behalf of the DLR Space Administration by the Federal Ministry of Economics and Technology of Germany.

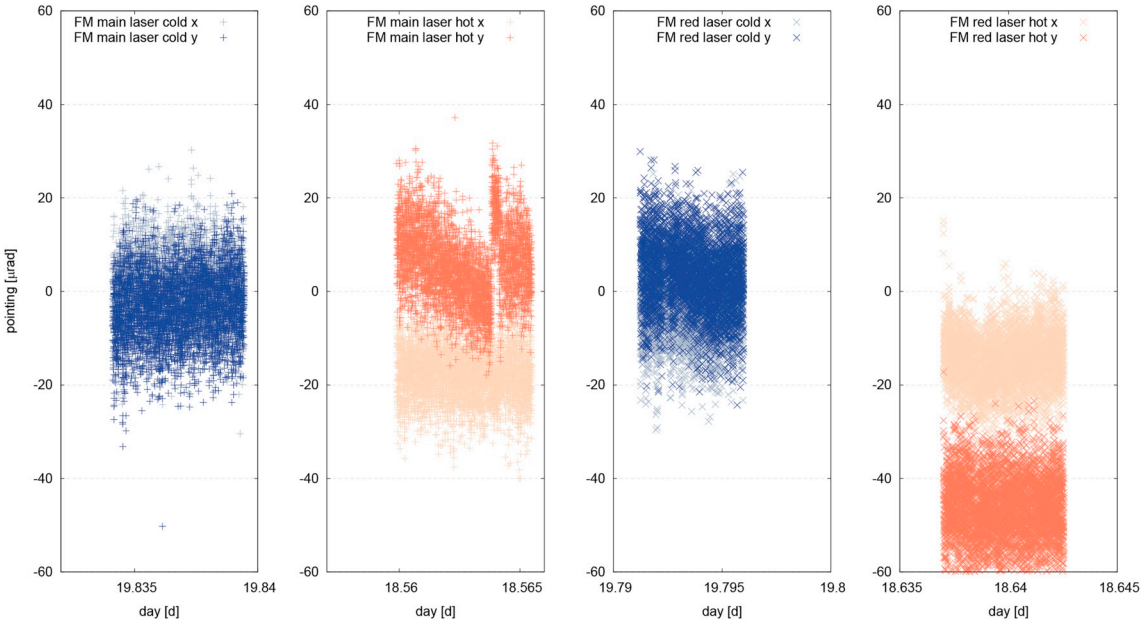

Fig. 20. Here the time resolved angular pointing is shown for the different temperature cases, hot and cold. The discontinuity was due to a wrongly placed aperture in the beam analysis software. This was considered during evaluation.

Appendix A. Notation

The following symbols are used in this paper

AEU	Analog Electronics Unit
APD	Avalanche Photodiode
APS	Application Software
AR	Anti Reflection
BELA	BepiColombo Laser Altimeter
BEX	Beam Expander
BOL	Begin of Life;
BPU	Baseplate Unit
CFRP	Carbon Fiber Reinforced Plastics
CMDVS	Control, Monitoring, Data Processing and Visualisation Software
CTE	Coefficient of Thermal Expansion
cw	continuous wave
DB	Database
DLR	Deutsches Zentrum fÃijr Luft-und Raumfahrt (German Aerospace Center)
DPM	Digital Processing Module
EGSE	Electric Ground Support Equipment
ELU	Electronics Unit
EOL	End of Life;
EQM	Engineering and Qualification Model
FS	Flight Spare
FM	Flight Model
FWHM	Full Width at Half Maximum
HW	Hardware
H/K	Housekeeping
LEU	Laser Electronics Unit
LHB	Laser Head Box
M − M	main-main (main DPM and PCM in ELU operate main laser in LHB)
MIS	Mercury Interface Simulator
MLA	Mercury Laser Altimeter
MLI	Multi Layer Insulation
MPO	Mercury Planetary Orbiter
Nd: *YAG*	Neodymium-doped Yttrium Aluminum Garnet;
OAP	Off-Axis Parabolic Mirror
PCM	Power Conversion Module
PFE	Power Front End
R − R	redundant-redundant (redundant DPM and PCM in ELU operate redundant laser in LHB)
RBU	Receiver Baffle Unit
RFM	Range Finder Module
RTL	Receiver Telescope
RX	Receiver
SESiLOX	Space Environment Simulation Facility for Laser and Optic Experiments
S/C	Spacecraft
SFE	Space Wire Front End
SNR	Signal to Noise Ratio
SPU	Straylight and Contamination Protection Unit
SW	Software
TBU	Transmitter Baffle Unit
TC	Telecommand;
TM	Telemetry
TSC	Text Script Console
TV	Thermal Vacuum
TX	Transmitter

References

[1] N. Thomas, T. Spohn, J.-P. Barriot, W. Benz, et al., The BepiColombo laser altimeter (BELA): concept and baseline design, Planet. Space Sci. 55 (10) (2007) 1398–1413 https://doi.org/10.1016/j.pss.2007.03.003 http://www.sciencedirect.com/science/article/pii/S0032063307000797.

[2] A. Milillo, M. Fujimoto, E. Kallio, S. Kameda, et al., The BepiColombo mission: an outstanding tool for investigating the Hermean environment, Planet. Space Sci. 58 (1) (2010) 40–60 comprehensive Science Investigations of Mercury: The scientific goals of the joint ESA/JAXA mission BepiColombo https://doi.org/10.1016/j.pss.2008.06.005 http://www.sciencedirect.com/science/article/pii/S0032063308001517.

[3] J.F. Cavanaugh, J.C. Smith, X. Sun, et al., The mercury laser altimeter instrument for the MESSENGER mission, Space Sci. Rev. 131 (1) (2007) 451–479, https://doi.org/10.1007/s11214-007-9273-4 https://doi.org/10.1007/s11214-007-9273-4.

[4] K. Seiferlin, S. Chakraborty, K. Gunderson, et al., Design and manufacture of a lightweight reflective baffle for the BepiColombo Laser Altimeter, Opt. Eng. 46 (2007), https://doi.org/10.1117/1.2722314 46 – 46 – 11 https://doi.org/10.1117/1.2722314.

[5] K. Gunderson, N. Thomas, M. Rohner, A laser altimeter performance model and its

application to BELA, IEEE Trans. Geosci. Rem. Sens. 44 (11) (2006) 3308–3319, https://doi.org/10.1109/TGRS.2006.880623.
[6] R. Kallenbach, E. Murphy, B. Gramkow, et al., Space-qualified laser system for the BepiColombo laser altimeter, Appl. Opt. 52 (36) (2013) 8732–8746, https://doi.org/10.1364/AO.52.008732 http://ao.osa.org/abstract.cfm?URI=ao-52-36-8732.
[7] Temperature and current accelerated lifetime conditions and testing of laser diodes for ESA BepiColombo space mission, Vol. 7918. doi:10.1117/12.874863. https://doi.org/10.1117/12.874863.
[8] C.S. Gardner, Ranging performance of satellite laser altimeters, IEEE Trans. Geosci. Rem. Sens. 30 (5) (1992) 1061–1072, https://doi.org/10.1109/36.175341.
[9] K. Seiferlin, S. Chakraborty, K.S. Gunderson, et al., Design and manufacture of a lightweight reflective baffle for the BepiColombo Laser Altimeter, Opt. Eng. 46 (2007), https://doi.org/10.1117/1.2722314 46 – 46 – 11 https://doi.org/10.1117/1.2722314.
[10] S.D. Togno, Thermal model and analysis of the BELA transmitter Stavroudis baffle in mercury orbit, European Workshop on Thermal and ECLS Software, 2009 https://elib.dlr.de/63391/.
[11] Y. Su, Thermal conductivity, phase stability, and oxidation resistance of Y3Al5O12 (YAG)/Y2O3–ZrO2 (YSZ) thermal–barrier coatings, Oxid. Metals 61 (3) (2004) 253–271, https://doi.org/10.1023/B:OXID.0000025334.02788.d3 https://doi.org/10.1023/B:OXID.0000025334.02788.d3.
[12] P. Chen, R. Hedgeland, L. Ramsey, R. Rivera, K. Houston, Contamination control of space-based laser instruments, Proc. SPIE 6291, Optical Systems Degradation, Contamination, and Stray Light: Effects, Measurements, and Control II, vol. 6291, SPIE, 2006.
[13] J. Gouman, T. Beck, M. Affolter, N. Thomas, et al., Measurement and stability of the pointing of the BepiColombo Laser Altimeter under thermal load, Acta Astronaut. 105 (1) (2014) 171–180 https://doi.org/10.1016/j.actaastro.2014.09.006 http://www.sciencedirect.com/science/article/pii/S0094576514003415.
[14] Spiricon, BeamGage User Guide, (2016) http://www.ophiropt.com/laser–measurement/sites/default/files/BeamGage-User-Guide-en.pdf.
[15] Y. Lee, Alignment of an off-axis parabolic mirror with two parallel He–Ne laser beams, Opt. Eng. 31 (11) (1992) 2287–2292 URL http://scitation.aip.org/getabs/servlet/GetabsServlet?prog=normal\&id=OPEGAR000031000011002287000001\&idtype=cvips\&gifs=yes.
[16] A. Hoffmann, Erstellen einer LabVIEW-Applikation zur Kanalisierung von Messdaten und Verifizierung der Messgenauigkeit des optischen AIV Testaufbaus fÃijr BELA, Master's thesis University of Applied Sciences Jena, August 2011.
[17] Crystalaser, Stabilized Compact Red Crystalaser, (2017) http://www.crystalaser.com/DL635-785.pdf.
[18] A. Cary, Beam Profiling: a Primer, Photon Inc. Member of the Ophir Group, https://www.ophiropt.com/user-files/laser/beam-profilers-/BP-tutorial-Photon.pdf.
[19] Z. Hui, L. Song, Y. Chi, The influence of elliptical Gaussian laser beam on inversion of terrain information for satellite laser altimeter, Photogramm. Eng. Rem. Sens. 82 (10) (2016) 767–773, https://doi.org/10.14358/PERS.82.10.767 http://www.ingentaconnect.com/content/asprs/pers/2016/00000082/00000010/art00012.
[20] S. Filin, B. Csatho, An Efficient Algorithm for the Synthesis of Laser Altimetry Waveforms, Planetary and Space Science. URL http://hdl.handle.net/1811/51702.
[21] J. Jingang Liu, D. Shen, S.-C. Tam, Y.-L. Lam, Modeling pulse shape of Q-switched lasers, IEEE J. Quant. Electron. 37 (7) (2001) 888–896, https://doi.org/10.1109/3.929588.